RSC Pharmaceutics

Accepted Manuscript

This article can be cited before page numbers have been issued, to do this please use: J. Jung, A. Sahu and G. Tae, *RSC Pharm.*, 2026, DOI: 10.1039/D6PM00162A.

ARTICLE Journal Name

Nanographene Oxide Enables Activity-Preserving Immobilization and Enhanced Stability of Galactose Oxidase

View Article Online
DOI: 10.1039/D6PM00162A

Junyoung Jung[a], Abhishek Sahu[a,b], and Giyoong Tae[a,*]

Received 00th January 20xx,
Accepted 00th January 20xx

DOI: 10.1039/x0xx00000x

Enzyme-mediated generation of reactive oxygen species (ROS) has attracted considerable interest for cancer-related applications. However, the biomedical use of oxidase enzymes is often limited by their intrinsic instability and rapid loss of catalytic activity under physiological conditions. Here, we report a nanographene oxide (nGO)-based platform that enables activity-preserving immobilization and stabilization of galactose oxidase (GaOX), a copper-containing oxidase that catalyzes hydrogen peroxide (H_2O_2) generation using D-galactose as a substrate. GaOX was physically immobilized onto nGO through non-denaturing interactions with high loading efficiency, followed by surface coating with Pluronic F127 to form a stable nanocomplex (F127@nGO-GaOX). Structural analysis confirmed that immobilized GaOX retained its secondary structure and catalytic parameters, including substrate affinity and catalytic efficiency. Notably, the immobilized enzyme exhibited markedly enhanced stability under serum-containing physiological conditions compared with the native enzyme. In addition, the F127@nGO-GaOX nanocomplex facilitated efficient cellular internalization, enabling intracellular ROS generation in the presence of galactose and resulting in enhanced cytotoxicity in cancer cells *in vitro*. These findings establish nGO as a nanocarrier-based formulation platform that preserves oxidase activity while improving enzyme stability and intracellular delivery. This work introduces GaOX as a ROS-generating therapeutic enzyme candidate and provides a simple strategy for developing enzyme-based formulations for biomedical applications.

Introduction

Enzymes, often referred to as biocatalysts, exhibit high catalytic efficiency and remarkable substrate specificity, making them valuable tools in biomedical, industrial, and environmental applications[1]. Despite these advantages, the practical use of enzymes in biomedical contexts is frequently limited by their intrinsic instability[2]. Exogenously administered enzymes are susceptible to structural denaturation and rapid activity loss under physiological conditions due to factors such as temperature fluctuations, pH variations, and proteolytic degradation[2,3]. In pathological microenvironments such as tumors and inflamed tissues, these challenges can be further exacerbated by elevated protease activity and local acidosis, which significantly compromise enzyme stability and functionality[4–6]. In addition, the inherent impermeability of enzymes across the cell membrane further restricts their intracellular applications.

To overcome these challenges, various strategies have been proposed to enhance the stability and functionality of enzymes for biomedical applications. Conjugation with biocompatible polymers, such as polyethylene glycol (PEG), has been widely employed to improve plasma half-life and modulate the biodistribution of enzymes[7,8]. However, polymer conjugation can introduce steric hindrance or induce conformational changes, potentially reducing catalytic activity[9]. Alternatively, nanomaterials-based immobilization or encapsulation strategies have been explored to improve enzyme stability while preserving catalytic function[10–12]. By providing a protective microenvironment and structural support, these platforms can enhance enzyme durability under biological conditions and potentially facilitate cellular delivery. Nevertheless, developing a simple formulation strategy that combines high enzyme loading, activity preservation, enhanced stability, and intracellular delivery remains challenging.

Nanographene oxide (nGO) is an interesting nanomaterial for enzyme immobilization[13]. The large specific surface area of nGO provides sufficient opportunities for the high amount of enzyme loading[13,14]. Additionally, the nGO surface contains many functional groups such as carboxyl (-COOH) and hydroxyl (-OH), which allow enzyme binding by various physical interactions such as hydrogen bonding, electrostatic interactions, hydrophobic associations, *etc*. As a result, graphene oxide has been widely investigated as a matrix for enzyme immobilization in applications ranging from biosensing and catalysis to environmental remediation[13–15]. Moreover, nGO has gained attention in biomedical fields such as drug delivery and tissue engineering owing to its favorable physicochemical properties and high loading capacity[16]. While nGO-based nanocarriers have demonstrated promising results for the delivery of anticancer drugs and photosensitizers[17,18], their potential as platforms for stabilizing and delivering functional enzymes for therapeutic contexts remains relatively underexplored.

Among oxidase enzymes, glucose oxidase (GOx) has been extensively investigated in cancer-related studies owing to its ability to generate hydrogen peroxide (H_2O_2) through glucose oxidation[19–21]. In this context, galactose oxidase (GaOX), a copper metalloenzyme that catalyzes the oxidation of D-galactose with concomitant H_2O_2 generation, may serve as a potential alternative oxidase enzyme. Despite its well-established catalytic properties and widespread use in biochemical and biosensing applications, the potential use of

[a] Department of Materials Science and Engineering, Gwangju Institute of Science and Technology (GIST), Gwangju 61005, Republic of Korea.
[b] Department of Biotechnology, National Institute of Pharmaceutical Education & Research (NIPER), Hajipur, 844102, India.

View Article Online
DOI: 10.1039/D6PM00162A

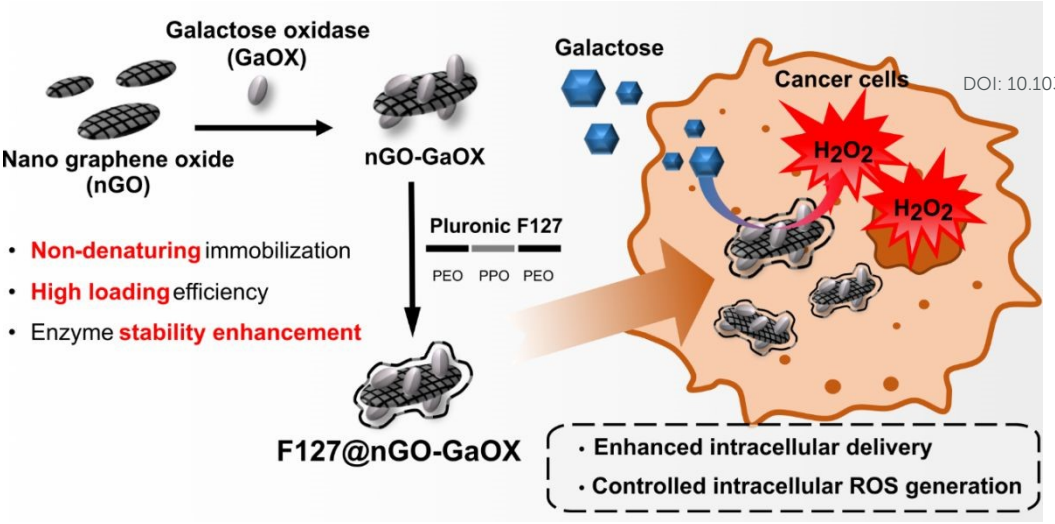

Figure 1. Schematic illustration of the F127@nGO-GaOX enzyme formulation platform for intracellular ROS generation. Galactose oxidase (GaOX) was physically loaded onto nanographene oxide (nGO) in a non-denaturing manner, followed by coating with Pluronic F127 to form F127@nGO-GaOX. The nanocomplex combines high-capacity enzyme loading, improved enzyme stability, and enhanced intracellular delivery while preserving GaOX catalytic activity. After cellular internalization, the delivered GaOX catalyzes D-galactose oxidation, leading to *in situ* hydrogen peroxide generation and enhanced intracellular ROS production.

GaOX as a functional enzyme in intracellular delivery or cancer-related biomedical contexts remains largely unexplored [22–26].

In this study, we introduce a nanographene oxide-based enzyme immobilization platform designed to stabilize GaOX while preserving its catalytic activity (**Figure 1**). GaOX was physically immobilized onto nGO through non-denaturing interactions, achieving high enzyme loading without detectable loss of catalytic activity or substrate affinity. The enzyme-loaded nanocomplex was subsequently coated with Pluronic F127 to improve colloidal stability under biological conditions, resulting in the formation of F127@nGO-GaOX. Importantly, the immobilized enzyme maintained its secondary structure and catalytic parameters while exhibiting significantly enhanced stability compared with free GaOX. Furthermore, the nGO-based nanocomplex facilitated efficient intracellular delivery of GaOX into cancer cells, enabling intracellular H_2O_2 generation in the presence of D-galactose. Collectively, this study demonstrates that nanographene oxide can serve as an effective platform for activity-preserving immobilization and stabilization of oxidase enzymes, and highlights the potential of GaOX as a functional ROS-generating enzyme for cancer-related applications.

Experimental

Materials & Methods

Materials

Graphene oxide was purchased from Angstron Materials (Dayton, OH, USA). Galactose oxidase was purchased from Worthington Biochemical (Lakewood, NJ, USA). Sodium hydroxide (NaOH), chloroacetic acid, D-galactose, horseradish peroxidase (HRP), azino-bis (3-ethylbenzothiazoline-6-sulfonic acid) liquid substrate (ABTS), and fluorescein isothiocyanate (FITC) were purchased from Sigma-Aldrich (Saint Louis, MO, USA). Pluronic F127 was a kind donation from BASF corporation (Seoul, Korea), and WST-8 assay reagent was purchased from Dojindo (Kumamoto, Japan). Dulbecco's Modified Eagle Medium (DMEM), fetal bovine serum (FBS), and antibiotic-antimycotic (AA) were purchased from Gibco (Grand Island, NY, USA). Hoechst 33342 and Micro BCA protein assay kit were purchased from Thermo Fisher Scientific (Waltham, MA, USA). Dihydroethidium (DHE) was purchased from Invitrogen (Carlsbad, CA, USA). Dialysis membrane (MWCO 3.5 kDa) was obtained from Spectrum Laboratories Inc. (Rancho Dominguez, CA, USA), and Nanosep OMEGA centrifugal filter system (MWCO 100 kD and 300 kD) was purchased from Pall Corporation (Port Washington, NY, USA).

Methods

Preparation of nanographene oxide (nGO)

Nanographene oxide was prepared by our previously reported method[27]. Briefly, graphene oxide (2.2 g) was dispersed in 20 mL of deionized water and heated at 70 ℃ with gentle stirring. Sodium hydroxide (200 mg) and chloroacetic acid (440 mg) were added to the graphene oxide solution, and the pH was adjusted to 10. The mixture was kept at 70 ℃ with gentle stirring for an overnight reaction. The reaction solution was centrifuged, and the supernatant was discarded. Reacted graphene oxide was dispersed in 20 mL of deionized water and sonicated using an ultrasonic probe (Vibra cell VCX740, Sonics & Materials Inc., Newtown, CT, USA) for 1 h. Sonicated graphene oxide solution was dialyzed (MWCO 3.5 kDa) for 1 day with frequent water changes. After dialysis, graphene oxide was further sonicated until the desired size was obtained. After ultrasonication, the nanographene oxide (nGO) solution was filtered with a 0.2 μm filter and stored at 4 ℃.

Preparation of F127@nGO-GaOX

To load galactose oxidase (GaOX), 500 µg of the enzyme was mixed with 100 µg of nGO in 500 µL of deionized water and gently rotated at 4 ℃ overnight. After incubation, the solution was put into a centrifugal filter (MWCO 300 kD) and centrifuged (2500 rpm, 4 ℃) to remove the unloaded GaOX. The upper part of the centrifugal filter containing the enzyme-loaded nGO (nGO-GaOX) was collected by adding 800 µL of DIW and pipetting for further Pluronic coating. The bottom part was used for assaying the loading efficiency of GaOX. Pluronic F127 (F127) (1 mg/100 µL in DIW) was added to the 800 µL of collected nGO-GaOX solution. The mixture was incubated at 100 rpm shaking at 37 ℃ for 2 h. The reacted solution was again purified by centrifugal filter (MWCO 100 kD) to remove unbound F127. The upper part of the filter containing Pluronic-coated, GaOX-loaded nGO (F127@nGO-GaOX) was collected and dispersed into PBS (pH 7.4) for further experiments. Solution collected from the bottom part of the centrifugal filter was used for measuring additional enzymes that might have been detached during the F127 coating.

Characterization of F127@nGO-GaOX

The hydrodynamic diameters and zeta potentials of nGO, nGO-GaOX, and F127@nGO-GaOX were measured by Dynamic Light Scattering (ELSZ, Otsuka Electronics Osaka, Japan). The morphology of nGO and F127@nGO-GaOX was analyzed by transmission electron microscopy (Tecnai G2 F30 S-Twin, FEI, Hillsboro, OR, USA). The loading efficiency of GaOX into the nGO was measured by the BCA protein assay. During the GaOX loading onto nGO and the Pluronic F127 coating to nGO-GaOX, the bottom part solutions in the centrifugal filter devices were used to measure the concentration of free GaOX through the BCA assay. The loading efficiency was calculated by measuring the amount of not-loaded GaOX and subtracting it from the initial amount of GaOX. The amount of F127 was estimated by measuring the mass of freeze-dried F127@nGO-GaOX and subtracting the known amounts of GaOX and nGO. To confirm the existence of all components in the nanocomplex, Fourier transform infrared (FTIR) spectra were measured (Vertex 70v, Bruker, Ettlingen, Germany). nGO, native GaOX, F127, nGO-GaOX, and F127@nGO-GaOX were lyophilized and compressed into discs for scanning from 4000 cm^{-1} to 600 cm^{-1}.

Analysis of colloidal and structural stability of nanocomplex

F127@nGO-GaOX was dispersed in PBS (pH 7.4) containing 10% FBS and was incubated at 37 ℃. The size of the nanocomplex was measured periodically by DLS to observe its colloidal stability.

FITC-labeled GaOX was used to measure the release of GaOX from the F127@nGO-GaOX. GaOX (3 mg) was mixed with FITC (0.3 mg), and the solution was stirred at room temperature overnight in a dark condition. The reacted solution was dialyzed (MWCO 3.5 kD) against deionized water for 24 h with frequent water changes to remove unreacted FITC. The FITC-conjugated GaOX solution was collected from the dialysis bag and freeze-dried for further experimentation.

FITC-GaOX was loaded onto nGO and further coated with Pluronic F127 to prepare F127@nGO FITC-GaOX. A dialysis system was prepared by putting a dialysis bag (MW 100kDa) in PBS (pH 7.4) containing 10% FBS. The prepared F127@nGO-FITC-GaOX was placed in the dialysis bag of the dialysis system, and the dialysis system was incubated at 37℃ with 100 rpm shaking. The PBS containing FITC-GaOX released from F127@nGO-FITC-GaOX was collected at 2, 4, 6, 12, 24, and 48 h, and the fluorescence signals were measured (ex: 495 nm, em: 520 nm). The enzyme release (%) was calculated using the following formula:

$$\text{Release}(\%) = \frac{\text{Fluorescence of released FITC} - \text{GaOX}}{\text{Fluorescence of loaded FITC} - \text{GaOX}} \times 100$$

To analyze the change in the secondary structures of loaded GaOX, the circular dichroism (CD) spectra of free GaOX, nGO-

GaOX, and F127@nGO-GaOX were measured by a CD spectrophotometer (J-815, Jasco Inc., Tokyo, Japan).

Analysis of enzyme kinetics and stability

Enzyme kinetics was analyzed through the oxidation of ABTS by HRP with H_2O_2 generated by the reaction of GaOX using D-galactose. ABTS (5.15 mg), galactose (1.8 mg), HRP (1 mg), and GaOX (1 mg) were dissolved in PBS (pH 7.4). Upon mixing these 4 solutions, the H_2O_2 generated by the reaction of D-galactose and GaOX was used to oxidize ABTS by HRP. The absorbance change of oxidized ABTS at 420 nm was measured at 37 ℃ for 10 min and later converted into the galactose concentration by Lambert-Beer law (ε = 43.2 $mM^{-1}cm^{-1}$)[28]. The Michaelis-Menten constant (K_m) and maximum velocity (V_{max}) were obtained by non-linear fitting of reaction rate versus substrate concentration using Origin software[29]. Turnover number (k_{cat}) and catalytic efficiency (k_{cat}/K_m) were calculated from the obtained K_m and V_{max}.

To determine the enzyme stability over time, F127@nGO-GaOX was dispersed in PBS (pH 7.4) containing 10% FBS and incubated at 37 ℃ for 48 h. GaOX activity was measured at various time points by the ABTS assay. The enzymatic activity was calculated based on GaOX units as defined by Paukner *et al.*, 2015 (28)[28]. Briefly, 1 unit of GaOX was the amount of enzyme necessary for the oxidation of 2 µmol ABTS per minute. The relative activity of F127@nGO-GaOX was calculated depending on the initial activity and compared with that of free GaOX.

The stability of enzymatic activity under acidic conditions was evaluated using acetate buffer (pH 4 and pH 5) and phosphate buffer (pH 6 and pH 7), which are suitable for maintaining the respective pH environments. F127@nGO-GaOX and free GaOX were incubated at 37 ℃ for 12 h in each buffer condition. After incubation, enzymatic activity was measured using the HRP/ABTS assay as described above. Activity retention under acidic conditions was assessed by calculating the activity ratio of F127@nGO-GaOX to free GaOX.

Analysis of *in vitro* cellular uptake

View Article Online
DOI: 10.1039/D5PM00263D

Cellular uptake of nanocomplex was analyzed using confocal laser scanning microscopy (FV1000, Olympus, Center Valley, PA, USA) and flow cytometry (FACS Caliber, BD Biosciences, San Jose, CA, USA). For confocal laser scanning microscopy measurements, glass coverslips were autoclaved and coated with gelatin solution. Then, the coverslips were placed in 12-well cell culture plates and cells (MCF-7 or SCC-7) were seeded at a density of 1×10^5 cells per well. After incubation with samples for 24 h, cells were washed with PBS and counterstained with Hoechst 33342. Then, cells were imaged by confocal microscopy.

For flow cytometry analysis, cells were seeded into a 12-well cell culture plate at a density of 2×10^5 cells per well. The next day, fresh media containing FITC-GaOX or F127@nGO-FITC-GaOX were added to the wells. After 24 h incubation, cells were washed, detached, collected, and analyzed by a flow cytometer.

Assay of *in vitro* ROS generation and cytotoxicity

Breast cancer cells (MCF-7) and squamous carcinoma cells (SCC-7) were cultured in DMEM supplemented with 10% FBS and 1% antibiotic-antimycotic. The cells were maintained in a 5% CO_2 incubator at 37 ℃.

To evaluate ROS generation induced by the reaction between GaOX and galactose, DHE staining was performed. MCF-7 or SCC-7 cells were seeded in 12-well cell culture plates at a density of 2×10^5 cells per well and incubated for 24 h. The cells were then treated with GaOX (1 μg/mL) and galactose (10 mM) for 4 h. After washing with PBS, the cells were incubated with DHE for 30 min. Nuclei were counterstained with Hoechst 33342 prior to fluorescence imaging using a fluorescence microscope (TE2000-U, Nikon, Tokyo, Japan).

Cytotoxicity was assessed using the WST-8 assay. Cytotoxicity was measured at various galactose concentrations while keeping the GaOX concentration fixed at 100 μg/mL. Cytotoxicity was also measured at various amounts of GaOX while keeping the galactose amount fixed at 40 mM. Briefly, MCF-7 cells or SCC-7 cells were seeded in 96-well cell culture plates at a density of 2×10^4 cells per well and incubated for 24 h. To analyze the cytotoxicity at various enzyme concentrations, the media were replaced with 50 μL of fresh media containing a fixed amount of galactose (80 mM) and 50 μL of fresh media containing various concentrations of GaOX or F127@nGO-GaOX. Also, to analyze the cytotoxicity at various substrate (galactose) concentrations, the media was replaced with 50 μL of fresh media containing a fixed amount of GaOX (200 μg/ml) or F127@nGO-GaOX (with the same GaOX amount) and 50 μL of fresh media containing various concentrations of galactose. 100 μL of fresh media was treated with cells as a control. After 24 h incubation, the culture media were removed, and the cells were washed with PBS. Then, 100 μL of media containing WST-8 reagent was added to each well and incubated at 37 ℃ for 1 h. After incubation, the absorbance at 450 nm was measured by a microplate reader (SpectraMax M2e, Molecular Devices, Sunnyvale, CA, USA), indicating the formazan production.

To evaluate whether the cytotoxicity induced by F127@nGO-GaOX was H_2O_2-dependent, a catalase rescue experiment was performed. SCC-7 cells were seeded in 96-well cell culture plates at a density of 1×10^4 cells per well and incubated for 24 h. The cells were then treated with F127@nGO-GaOX (25 μg/mL in terms of GaOX), galactose (20 mM), and/or catalase (100 U/mL) according to each experimental group and incubated for an additional 24 h. Catalase was used as an H_2O_2 scavenger. After incubation, the culture supernatants were collected and subjected to an Amplex UltraRed/HRP assay to quantify H_2O_2 generation. Fluorescence was measured at excitation and emission wavelengths of 550 and 580 nm, respectively, using a microplate reader (Varioskan Lux, Thermofisher, Waltham, MA, USA). The remaining cells were washed with PBS and then subjected to the WST-8 assay as described above.

Results and Discussion

Preparation and Characterization of F127@nGO-GaOX

The hydrodynamic size and zetapotential of the nanocomplexes were analyzed by dynamic light scattering (DLS) (**Figure 2A**, **2B,** and **Table 1**). The average hydrodynamic size of the nGO prepared *via* ultrasonication was 52 ± 7 nm. After GaOX loading onto nGO through physical interactions, the average particle size increased to 81 ± 2 nm. Subsequent coating with Pluronic F127 (F127) did not result in a significant further increase in size, with F127@nGO-GaOX exhibiting an average hydrodynamic size of 82 ± 2 nm. In contrast, the surface charge showed a pronounced change upon F127 coating. The zeta potential of nGO-GaOX (-69.57 ± 4.71 mV) increased significantly to -17.77 ± 4.31 mV after F127 coating, indicating successful surface modification. Notably, when nGO was coated with F127 in the absence of GaOX (F127@nGO), the zeta

Table 1. Size, PDI, and zeta potential of nGO, F127 nGO, nGO-GaOX, and F127@nGO-GaOX.

	Diameter (nm)	PDI	Zeta Potential (mV)
nGO	52 ± 7	0.244 ± 0.008	− 70.78 ± 1.34
F127@nGO	55 ± 7	0.200 ± 0.074	− 26.85 ± 4.51
nGO-GaOX	81 ± 2	0.262 ± 0.005	− 69.57 ± 4.71
F127@nGO-GaOX	82 ± 2	0.242 ± 0.006	− 17.77 ± 4.31

View Article Online
DOI: 10.1039/D6PM00162A

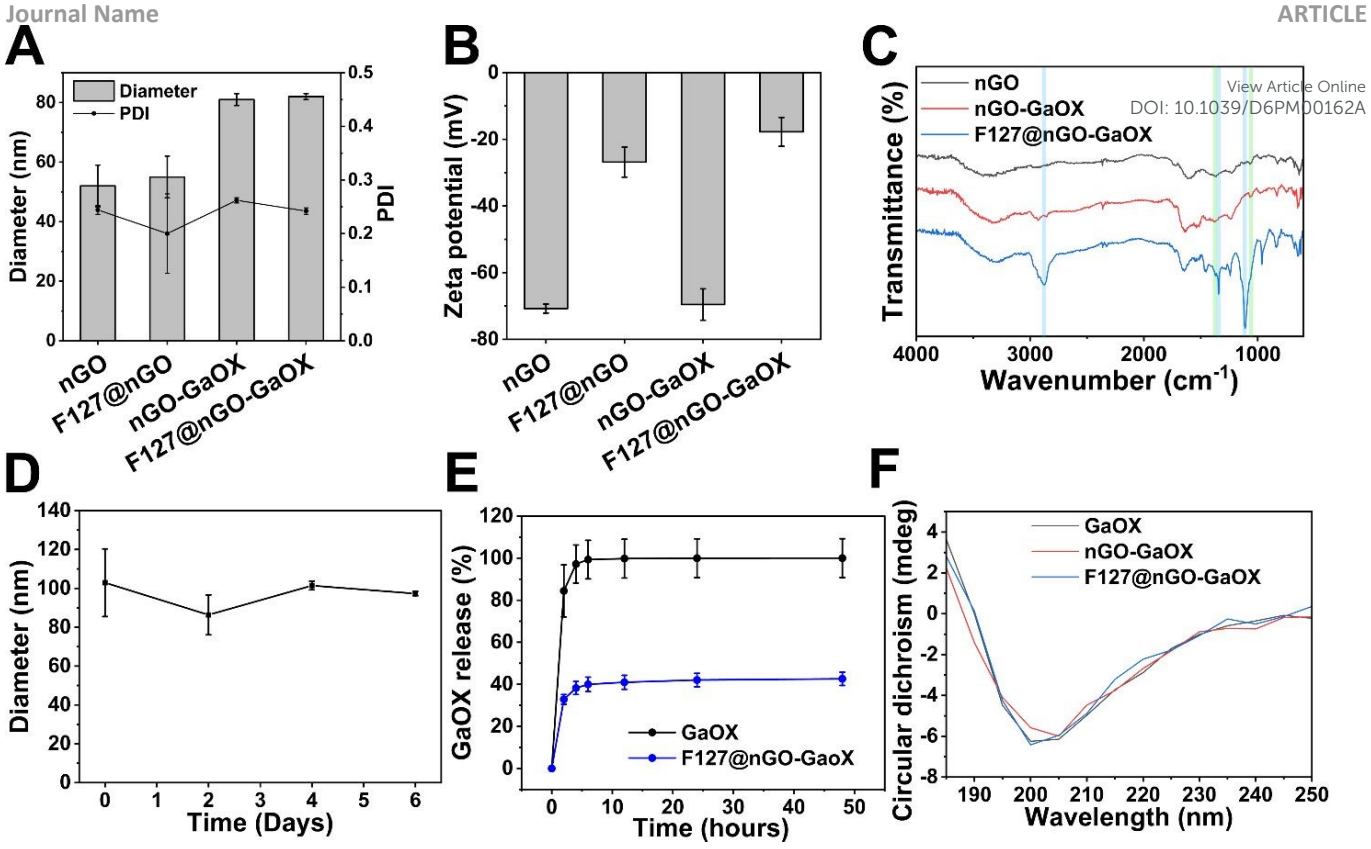

Figure 2. (A) Size and PDI, and (B) zeta potential of nGO, F127@nGO, nGO-GaOX, and F127@nGO-GaOX in DIW. (C) FTIR spectra of nGO (black), nGO-GaOX (red), F127@nGO-GaOX (blue). The green boxes highlight characteristic peaks of enzymes at 1050 cm^{-1} (amide Ⅰ bond) and 1415 cm^{-1} (amide Ⅱ bond). The blue boxes highlight characteristic absorption peaks of F127 at 2883 cm^{-1} (C-H stretching), 1342 cm^{-1} (O-H bend), and 1106 cm^{-1} (C-O-C stretching vibration). (D) Average size of F127@nGO-GaOX in PBS (pH 7.4) containing 10% FBS incubated at 37 ℃. (E) Release of GaOX from F127@nGO-GaOX in PBS (pH 7.4) containing 10% FBS. (F) Circular dichroism spectra of GaOX (black), nGO-GaOX (red), and F127@nGO-GaOX (blue).

potential increased markedly from -70.78 ± 1.34 mV to -26.85 ± 4.51 mV. This pronounced change in surface charge further confirms that the increased zeta potential observed for F127@nGO-GaOX originates from the presence of the F127 coating on the nGO surface. Such masking of the negative surface charge of nGO by F127 aligns with previous reports[17,30]. Therefore, these results indicate that F127 was successfully and thinly coated on the surface of the nGO-GaOX system.

The morphology of the prepared nGO and F127@nGO-GaOX was analyzed by transmission electron microscopy (**Figure S1**). The hydrodynamic sizes determined by DLS were consistent with the particle sizes observed in the TEM images. In particular, the presence of a faint surrounding layer observed exclusively in F127@nGo-GaOX indicates successful coating of GaOX and F127 on the nGO surface. This morphological feature is consistent with previously reported observations for F127-coated nGO systems[27].

The loading amount of GaOX was determined by subtracting the amount of unloaded enzyme, separated using a centrifugal filter, from the initial GaOX quantity. The total enzyme content loaded onto F127@nGO-GaOX was measured to be 322 ± 14 μg, which was ~3.2-fold higher than the amount of nGO (100 μg). The enzyme loading efficiency was calculated to be 65 ± 3%. This remarkable enzyme loading capacity and efficiency can be attributed to the extensive surface area of nGO. This surface area not only accommodates ample enzyme binding space but also fosters various physical interactions, including hydrogen bonding, hydrophobic associations, π-π interactions, and electrostatic interactions[28]. The final composition of F127@nGO-GaOX was determined to be 12.4 ± 0.8% nGO, 40.3 ± 3.9% GaOX, and 40.2 ± 6.8% F127 (**Table 2**). These results are consistent with the zeta potential change observed in **Figure 2B**, confirming the successful coating of F127 on the nanocomplex.

The FTIR spectra confirmed the presence of nGO, GaOX, and F127 in F127@nGO-GaOX (**Figure 2C** and **Figure S2**). nGO exhibited distinctive features, including a broad peak at approximately 3445 cm^{-1} (O-H stretching), 2923cm^{-1} (C-H bonding), 1220cm^{-1}, and 1020 cm^{-1} (C=O and C-O stretching)[31]. GaOX displayed characteristic peaks at 1050 cm^{-1} and 1415 cm^{-1}, corresponding to amide I and amide II bonds, respectively. F127's presence was marked by peaks at 2883 cm^{-1} (C-H stretching), 1342 cm^{-1} (O-H bend), and 1106 cm^{-1} (C-O-C stretching vibrations)[32]. As illustrated in **Figure 2C**, F127@nGO-GaOX exhibited characteristic peaks associated with all of these components.

To confirm the *in vitro* colloidal stability of F127@nGO-GaOX in physiological conditions, its size in PBS containing 10% FBS was analyzed (**Figure 2D**). The average size of F127@nGO-GaOX on both day 1 and day 6 remained consistent at 103 ± 17 nm and 97 ± 1nm, respectively, indicating the absence of

View Article Online
DOI: 10.1039/D6PM00162A

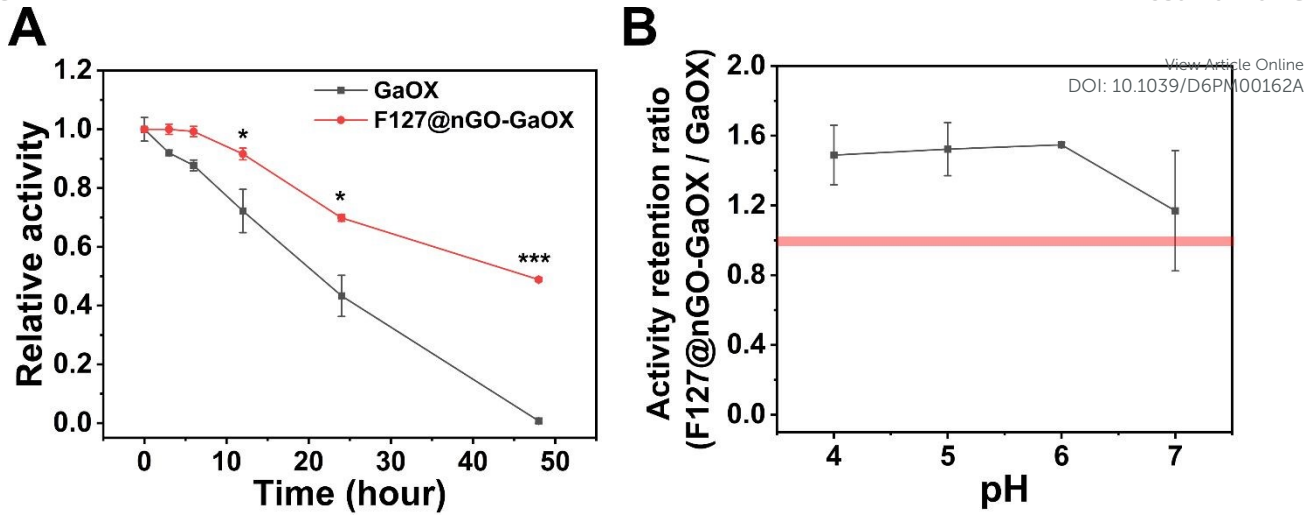

Figure 3.(A) Stability of enzymatic activity of GaOX and F127@nGO-GaOX incubated at 37 ℃ in PBS (pH 7.4) containing 10% FBS. (B) Relative activity retention expressed as the activity ratio of F127@nGO-GaOX to native GaOX at each pH after 12 h incubation. The red shaded region indicates a ratio of 1, representing no difference in activity between F127@nGO-GaOX and GaOX. Enzymatic activity was measured using an HRP/ABTS assay with galactose as the substrate. Statistical significance: #p>0.05, * p<0.05, **p<0.01, ***p<0.001.

nanocomplex aggregation. In contrast, nGO-GaOX without the F127 coating immediately precipitated in the buffer solution (**Figure S3**). Therefore, the F127 coating effectively prevented nanoparticle aggregation. Notably, the slight difference in the hydrodynamic size of F127@nGO-GaOX observed between **Figure 2A** and **Figure 2D** can likely arise from the use of different dispersion solvents during measurement, namely DIW for **Figure 2A** and PBS containing 10 % FBS for **Figure 2D**.

Given that GaOX was immobilized onto nGO through physical interactions, the possibility of enzyme leaching from the nanocomplex could not be excluded. To assess this, the release behavior of GaOX from F127@nGO-GaOX was investigated *in vitro* using FITC-labeled GaOX (**Figure 2E**). The amount of released enzyme was quantified by measuring the fluorescence intensity of FITC-GaOX. An initial burst release of 32.8 ± 2.3% was observed within the first 2 h, followed by a slower and sustained release phase, gradually reaching ~43 % cumulative release at 48 h. Considering that GaOX was initially loaded at ~3.2-fold excess relative to nGO, more than two-thirds of the enzyme remained associated with the nanocomplex even after 48 h. These results indicate that F127@nGO-GaOX exhibits efficient enzyme loading and stable retention of GaOX under serum-containing *in vitro* conditions.

Enzyme loading or immobilization within nanomaterials can potentially lead to conformational changes, resulting in reduced or lost catalytic activity[29]. To assess this possibility, the secondary structures of GaOX before and after loading onto nGO were analyzed using CD spectroscopy. The CD spectra of GaOX, nGO-GaOX, and F127@nGO-GaOX exhibited highly similar profiles (**Figure 2F**), indicating that the secondary structure of GaOX was well preserved upon immobilization onto nGO as well as after subsequent F127 coating.

The successful immobilization of GaOX onto nGO can be attributed to the physicochemical characteristics of nanographene oxide, particularly its large specific surface area and the presence of abundant oxygen-containing functional groups. These surface functionalities enable multiple non-covalent interactions, including hydrogen bonding, electrostatic interactions, and hydrophobic associations with protein molecules. Such interactions allow enzyme adsorption while minimizing structural perturbation of the protein. The preservation of GaOX secondary structure observed in the CD spectra further supports that the immobilization process occurs under non-denaturing conditions.

Notably, the high enzyme loading capacity observed in this study (~3.2-fold higher than the mass of nGO) highlights the advantage of the two-dimensional structure of graphene oxide for enzyme immobilization. The large accessible surface area allows multiple enzyme molecules to adsorb without severe steric hindrance, which likely contributes to the retention of catalytic activity after immobilization. In addition, the F127 coating effectively stabilized the nanocomplex under physiological conditions, preventing aggregation of the graphene oxide sheets while maintaining enzyme accessibility to the substrate. These results demonstrate that nGO can serve as an effective nanocarrier-based formulation platform for enzyme delivery by integrating high-capacity loading, structural

Table 2. Weight composition of nGO, GaOX, and F127 in the F127@nGO-GaOX

nGO (%)	GaOX (%)	F127 (%)
12.4 ± 0.8	40.3 ± 3.9	40.2 ± 6.8

View Article Online
DOI: 10.1039/D6PM00162A

preservation, catalytic activity retention, and colloidal stability under biologically relevant conditions.

Enzyme kinetics and stability of enzymatic activity

In this study, GaOX was physically immobilized onto nGO. Enzyme immobilization within nanomaterials can potentially alter catalytic properties and stability[33–35]. Therefore, the enzyme kinetics and stability of GaOX were analyzed before and after loading onto nGO (**Figure 3** and **Table 3**). GaOX catalyzes the oxidation of the primary alcohol group of D-galactose to the corresponding aldehyde derivative in the presence of molecular oxygen, concomitantly producing H_2O_2 as a byproduct[36,37]:

$$\text{D-galactose} + O_2 \rightarrow \text{oxidized D-galactose} + H_2O_2$$

To evaluate GaOX-mediated H_2O_2 generation and catalytic activity, an HRP/ABTS-coupled colorimetric assay was employed[28]. In this assay, H_2O_2 produced by the GaOX-catalyzed oxidation of D-galactose is used by HRP to oxidize ABTS, generating a colored product that can be monitored by measuring absorbance at 420 nm. Thus, the HRP/ABTS system enables quantitative assessment of GaOX-mediated H_2O_2 generation and enzymatic activity.

The kinetic parameters of free GaOX were determined as follows: a maximum initial velocity (V_{max}) of $2.37 \times 10^{-3} \pm 3.0 \times 10^{-4}$ mM/s, a Michaelis-Menten constant (K_m) of 39.0 ± 2.4 mM, a catalytic constant (k_{cat}) of 154.1 ± 19.2 s^{-1}, and a catalytic efficiency (k_{cat}/K_m) of 3.95 ± 0.37 $mM^{-1}s^{-1}$. In comparison, F127@nGO-GaOX exhibited a V_{max} of 2.41 x 10^{-3} ± 1.2 x 10^{-4} mM/s, a K_m of 39.6 ± 1.6 mM, a k_{cat} of 156.9 ± 8.1 s^{-1}, and a k_{cat}/K_m of 3.96 ± 1.59 $mM^{-1}s^{-1}$. These results indicate that no significant changes occurred in the kinetic parameters of GaOX following immobilization onto nGO and subsequent F127 coating, suggesting that the physical loading process did not adversely affect the catalytic properties of the enzyme.

For enzyme immobilization, the functionally active enzyme fraction is more important than total protein mass alone. Therefore, the BCA-derived GaOX loading was further evaluated by quantitative enzymatic activity analysis. After removal of unbound GaOX, purified F127@nGO-GaOX was adjusted to the same GaOX-equivalent concentration as free GaOX based on BCA quantification and subjected to ABTS/HRP-based kinetic analysis. The K_m, k_{cat}, and k_{cat}/K_m values of F127@nGO-GaOX were almost the same as those of free GaOX, supporting that the BCA-estimated GaOX loading is consistent with catalytically active GaOX retained in the final nanocomplex.

Although enzyme immobilization can potentially induce steric hindrance and reduce substrate accessibility[38], several studies have reported preserved or even enhanced enzymatic reaction parameters and the preservation of enzyme secondary structure after immobilization onto graphene oxide. Monajati *et al.*, 2018 (39) confirmed that the enzymatic reaction kinetic constants of L-asparaginase remained unchanged after physically loading it onto graphene oxide nanosheets[39]. Bolibok *et al.*, 2017 (40) observed that the maximum initial velocity and Michaelis-Menten constant of catalase could increase or decrease after physical immobilization onto nGO, depending on the loaded amount of catalase[40]. They also noted that by loading a substantial amount of catalase, changes in the enzyme's secondary structure were minimized. In our system, the loading amount of GaOX onto nGO was over 3 times the nGO amount. This substantial loading of GaOX onto nGO likely contributed to maintaining enzyme reaction kinetics parameters and the secondary structure of GaOX. In summary, the same substrate affinity and catalytic efficiency as those of free GaOX could be obtained from F127@nGO-GaOX.

One major limitation of biological enzymes is their poor stability under physiological conditions, particularly in serum-containing environments where proteolytic degradation readily occurs[41]. To evaluate the stability of GaOX under serum conditions, the enzymatic activity of free GaOX and F127@nGO-GaOX was compared (**Figure 3A**). Both samples were dispersed in PBS (pH 7.4) containing 10% FBS and incubated at 37 ℃ for up to 48 h. After incubation, free GaOX completely lost its enzymatic activity, whereas GaOX immobilized within F127@nGO-GaOX retained ~49% of its initial activity. These results demonstrate that the combined effects of physical immobilization on nGO and surface coating with F127 markedly enhance the stability of GaOX in serum-containing environments, effectively protecting the enzyme from deactivation under physiological conditions.

Each enzyme exhibits an optimal pH range, and a pronounced decrease in catalytic activity is generally observed when the pH deviates from this optimum. For GaOX, the optimal pH has been reported to be around pH 7.0, and a substantial loss of activity under acidic conditions, such as those characteristic of the tumor microenvironment, has been previously reported[28]. To explore the potential applicability of GaOX in cancer-related

Table 3. Enzyme kinetics parameters of GaOX and F127@nGO-GaOX, calculated based on a Michaelis-Menten model. There was no statistical difference between GaOX and F127@nGO-GaOX.

	V_{max} (mM/s)	K_m (mM)	E_t (mM)	k_{cat} (s^{-1})	k_{cat} / K_m (mM^{-1} s^{-1})
GaOX	$2.37 \times 10^{-3} \pm 3.0 \times 10^{-4}$	39.0 ± 2.4	1.54×10^{-5}	154.1 ± 19.2	3.95 ± 0.37
F127@nGO-GaOX	$2.41 \times 10^{-3} \pm 1.2 \times 10^{-4}$	39.6 ± 1.6	1.54×10^{-5}	156.9 ± 8.1	3.96 ± 1.59

View Article Online
DOI: 10.1039/D6PM00162A

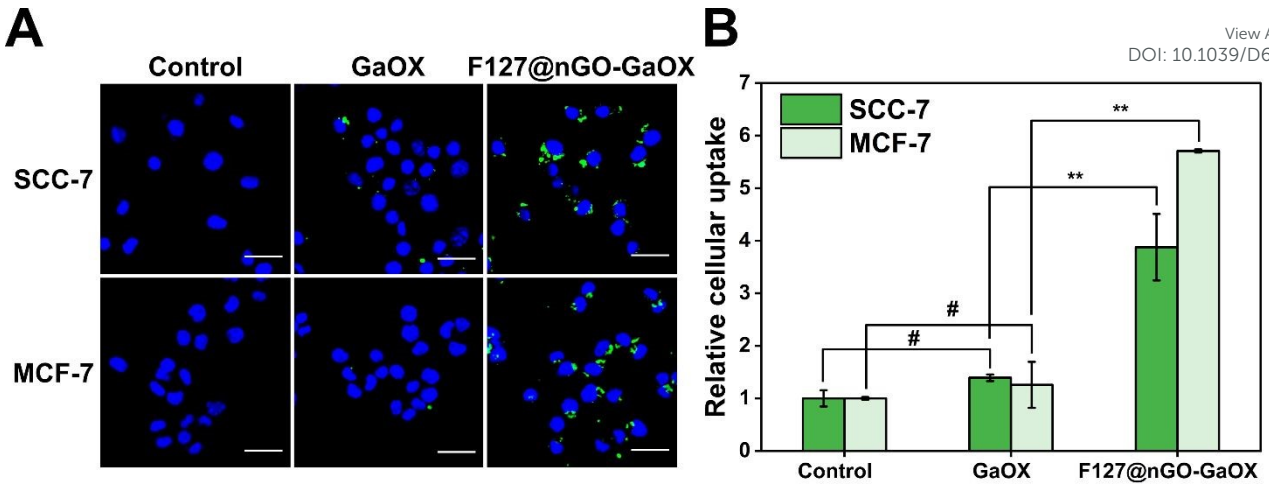

Figure 4. Enhanced cell uptake of F127@nGO-GaOX. (A) Confocal images of MCF-7 cells and SCC-7 cells treated with PBS (control), FITC-GaOX, and F127@nGO-FITC-GaOX, respectively. Blue: Hoechst, Green: FITC. Scale bar: 30 μm. (B) Quantification of the cell uptake of FITC-GaOX or F127@nGO-FITC-GaOX using flow cytometry. Statistical significance: #p>0.05, * p<0.05, **p<0.01.

contexts, we investigated the extent to which its enzymatic activity could be retained under acidic conditions (**Figure 3B**). To isolate the effect of pH, all measurements were conducted in serum-free buffer systems. As expected, no significant difference in enzymatic activity was observed between free GaOX and F127@nGO-GaOX at pH 7.0, which is close to the reported optimal pH of GaOX. In contrast, at acidic pH values (pH 4, 5, and 6), F127@nGO-GaOX consistently exhibited ~1.5-fold higher enzymatic activity compared to free GaOX. These results indicate that the F127@nGO-GaOX platform can partially preserve the catalytic activity of GaOX under acidic conditions. This enhanced activity retention under low-pH environments suggests that immobilization within the F127@nGO-GaOX nanocomplex may improve the feasibility of applying GaOX in cancer-related therapeutic settings.

In many graphene oxide-based enzyme immobilization systems, enzymes are covalently linked to the GO surface through chemical coupling reactions to prevent enzyme leaching and improve long-term stability[42]. Although such covalent immobilization can provide strong enzyme attachment, chemical modification of the enzyme or support surface may also affect the native enzyme conformation, alter substrate accessibility, or reduce catalytic activity[43]. In contrast, the present system achieved efficient GaOX immobilization through physical interactions without chemical crosslinking or covalent conjugation. This physical immobilization is likely mediated by multiple weak interactions between GaOX and the nGO surface, including hydrophobic interactions, π-π interactions, hydrogen bonding, and electrostatic interactions. Such multivalent but non-covalent interactions may allow GaOX adsorption while minimizing structural perturbation important for maintaining enzymatic function.

Despite the non-covalent loading strategy, F127@nGO-GaOX exhibited a high enzyme loading efficiency, stable enzyme retention under serum-containing conditions, and markedly improved enzymatic stability compared to free GaOX. Importantly, CD spectral analysis and enzyme kinetic measurements demonstrated that the secondary structure, substrate affinity, and catalytic efficiency of GaOX were preserved after immobilization. These findings indicate that nGO can serve not merely as a passive enzyme carrier but as an activity-preserving immobilization matrix that stabilizes GaOX while maintaining its native catalytic function. Therefore, the physical immobilization strategy used in this study provides a simple and chemically mild alternative to covalent enzyme immobilization on graphene oxide-based platforms.

Within the scope of the present analysis, CD spectroscopy supports the preservation of GaOX secondary structure, while the kinetic data indicate retention of substrate affinity and catalytic function after immobilization. Although the tertiary structure and the full extent of enzyme denaturation were not directly analyzed, these results suggest that the mild physical immobilization strategy used here can preserve the enzymatic function of GaOX under the formulation conditions used in this study. Accordingly, the activity-preserving effect observed here is best interpreted in the context of GaOX, as the outcome of enzyme immobilization may vary depending on enzyme-specific properties.

In vitro cellular uptake of GaOX and F127@nGO-GaOX

Various studies have demonstrated that nano-sized graphene oxide can readily enter cells[44–46]. Mu *et al.*, 2012 (45) analyzed the size-dependent cell uptake of protein-coated nano-sized graphene oxide. They found that small-sized protein-coated graphene oxide initially adheres to the cell membrane and is subsequently internalized by clathrin-mediated endocytosis[45]. In addition, Xu *et al.*, 2014 (46) reported that PEGylated graphene oxide effectively delivered paclitaxel into cancer cells, leading to enhanced cytotoxicity compared with free paclitaxel[46]. Furthermore, the coating of nanomaterials with Pluronic compounds can influence cellular nanoparticle uptake.

View Article Online
DOI: 10.1039/D6PM00162A

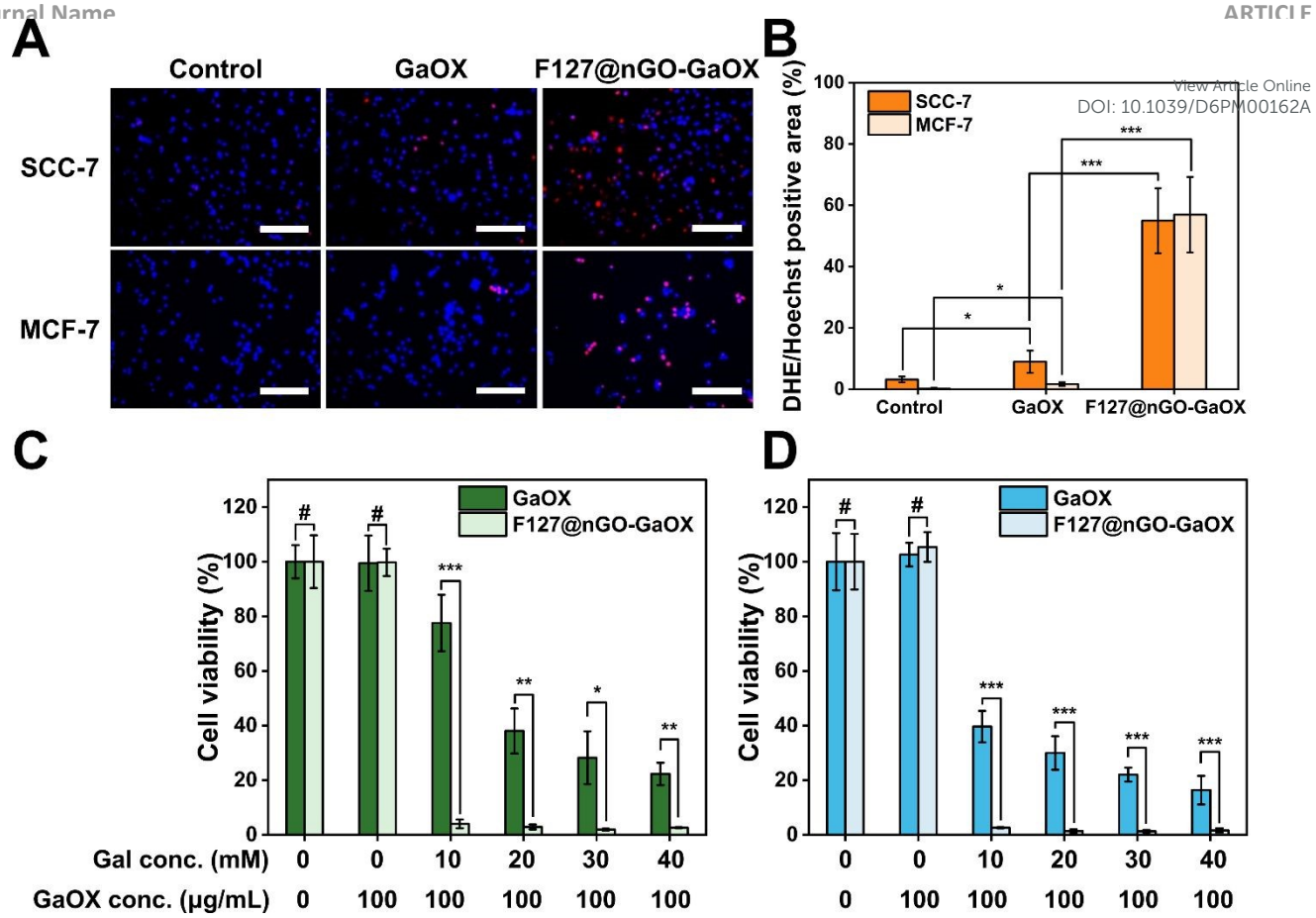

Figure 5. *In vitro* ROS generation and cytotoxicity induced by GaOX and F127@nGO-GaOX in cancer cells. (A) Representative DHE staining images and (B) quantification using 5 individual images. Viability of (C) SCC-7 and (D) MCF-7 cells at various galactose concentrations with a fixed GaOX concentration (100 μg/mL) measured by WST-8 assay. Statistical significance: # p >0.05, *p<0.05, **p<0.01, ***p<0.001.

Yan *et al.*, 2010 (47) confirmed that Pluronic F68 coating on PLGA nanoparticles increased their uptake by cancer cells compared to uncoated PLGA nanoparticles[47].

To assess the cellular uptake of GaOX and F127@nGO-GaOX in both MCF-7 and SCC-7 cells, FITC-labeled GaOX was utilized to prepare F127@nGO-FITC-GaOX. After the administration of FITC-GaOX and F127@nGO-FITC-GaOX to cells, cellular uptake was visualized using confocal laser scanning microscopy (**Figure 4A**) and quantified through flow cytometry (**Figure 4B**). As shown in **Figure 4B**, in both MCF-7 and SCC-7 cells, FITC-GaOX exhibited negligible cellular uptake, showing no significant difference compared to the negative control group (PBS only). In contrast, F127@nGO-FITC-GaOX demonstrated a ~2.8-fold increase in SCC7 cells and a ~4.5-fold increase in cellular uptake in MCF-7 cells compared to FITC-GaOX. Therefore, it can be concluded that free GaOX has limited efficiency in crossing the cell membrane, while GaOX can be effectively delivered into cells when loaded onto the nanocomplex. This trend was also consistently observed in confocal laser scanning microscopy images (**Figure 4A**).

In vitro ROS generation and cytotoxicity

GaOX catalyzes the oxidation of D-galactose by converting primary alcohols to aldehydes, during which molecular oxygen is reduced to H_2O_2[48]. As H_2O_2 is a key mediator of oxidative cytotoxicity, the subcellular location of ROS generation is expected to critically influence therapeutic efficacy. In ROS-based therapeutic strategies, extracellularly generated ROS can also contribute to tumor cell damage. However, the therapeutic efficiency differs depending on whether ROS are generated extracellularly or intracellularly[49]. Intracellular ROS generation can induce rapid and direct damage to DNA, lipids, and proteins, thereby effectively promoting tumor cell death[50]. Although H_2O_2 exhibits relatively high membrane permeability compared to other ROS, the biological impact of intracellularly generated H_2O_2 is expected to differ from that of extracellularly produced H_2O_2 in the context of tumor cell eradication. These differences arise from the proximity of intracellular ROS to vital cellular components and signaling pathways. Therefore, efficient intracellular delivery of ROS-generating systems represents a meaningful strategy to enhance therapeutic efficacy.

To examine whether the enhanced cellular uptake of F127@nGO-GaOX observed in **Figure 4** is associated with increased oxidative stress in cancer cells, DHE staining was performed following treatment with GaOX and galactose (**Figures 5A, 5B, S4, and S5**). DHE staining reflects increased intracellular ROS levels, as oxidized DHE derivatives intercalate into nuclear DNA, resulting in prominent nuclear fluorescence.

In both SCC-7 and MCF-7 cells, DHE fluorescence was markedly increased in the F127@nGO-GaOX-treated groups

compared to those treated with free GaOX, following co-treatment with D-galactose. Although enzyme stability in serum-containing media is expected to contribute to this difference, considering the relatively short incubation time of 4 h, the enhanced DHE signal can also be reasonably attributed to increased intracellular ROS generation mediated by F127@nGO-GaOX. Therefore, under the current *in vitro* conditions, these results indicate that F127@nGO-GaOX induces substantial oxidative stress in cancer cells through its improved stability and enhanced cellular uptake. Given the significantly enhanced cellular uptake of F127@nGO-GaOX observed in **Figure 4,** the increased DHE signal is likely associated with ROS generation mediated by the internalized nanocomplex rather than solely by extracellularly generated H_2O_2. Although DHE staining is commonly used to indicate intracellular oxidative stress, it does not specifically distinguish individual ROS species. Considering the catalytic mechanism of GaOX, the increased DHE signal observed in this study is likely associated with intracellular oxidative stress induced by H_2O_2 generated from the enzymatic reaction.

To evaluate the *in vitro* anticancer effect of H_2O_2 generated by GaOX in the presence of galactose, mouse squamous carcinoma SCC-7 cells and human breast cancer MCF-7 cells were treated with GaOX or F127@nGO-GaOX, along with galactose. The metabolic activity was then measured and compared with a positive control group (no treatment) to assess cytotoxicity (**Figures 5C, 5D,** and **S6**).

Initially, neither GaOX nor F127@nGO-GaOX exhibited cytotoxicity when applied alone to both SCC-7 and MCF-7 cells, indicating the nanocomplex without its substrate was safe and non-toxic (**Figure 5C** and **5D**). Similarly, treatment with galactose, the substrate for GaOX, did not affect the viability of SCC7 and MCF7 cells, as expected (**Figure S6**). However, when the cells were exposed to various galactose concentrations (10, 20, 30, and 40 mM) at a fixed GaOX concentration of 100 μg/mL, metabolic activity decreased in a dose-dependent manner. Notably, when treated with F127@nGO-GaOX, cells exhibited significantly higher cytotoxicity compared to free GaOX at the same galactose concentration.

Likewise, in cells treated with GaOX concentrations of 25, 50, 100, and 150 μg/mL, along with 40 mM galactose, a dose-dependent reduction in metabolic activity was observed compared to the positive control group (**Figure S6**). Notably, F127@nGO-GaOX, at the same GaOX concentration, displayed substantially greater cytotoxicity than free GaOX. This result highlights the significantly enhanced *in vitro* cytotoxicity of F127@nGO-GaOX when combined with galactose, as compared to native GaOX with galactose.

To further evaluate whether the oxidative stress and cytotoxicity induced by F127@nGO-GaOX were associated with GaOX-mediated H_2O_2 production, a catalase rescue analysis was performed (**Figure S7**). When SCC-7 cells were treated with F127@nGO-GaOX and galactose, marked cytotoxicity was observed, whereas co-treatment with catalase restored cell viability to a level comparable to that of the control group (**Figure S7A**). This result indicates that catalase, an H_2O_2-scavenging enzyme, effectively decomposed the H_2O_2 generated by the F127@nGO-GaOX/galactose system and thereby protected the cells from oxidative damage. In addition, H_2O_2 generation in the culture supernatant was directly evaluated using the H_2O_2-responsive Amplex UltraRed/HRP assay. The F127@nGO-GaOX with a galactose group showed a pronounced increase in fluorescence signal, whereas catalase co-treatment markedly reduced the signal (**Figure S7B**). Notably, the catalase-only-treated group showed a lower fluorescence signal than the untreated control, suggesting that catalase also scavenged basal H_2O_2 present in the cellular environment. Taken together, these results support that the oxidative stress and cytotoxicity observed in **Figure 5** were mainly mediated by GaOX-dependent H_2O_2 generation.

These findings suggest that improving the intracellular delivery of ROS-generating enzymes represents an effective strategy to amplify oxidative stress within cancer cells. Since free GaOX showed limited cellular uptake, its cytotoxic effect was likely mediated mainly by extracellular H_2O_2 generation. In contrast, F127@nGO-GaOX was efficiently internalized into cancer cells, enabling more effective intracellular H_2O_2 generation in the presence of D-galactose. Thus, the enhanced cytotoxicity of F127@nGO-GaOX can be attributed to the combined effects of improved enzyme stability and intracellular delivery.

Overall, this study presents F127@nGO-GaOX as a simple enzyme-based nanomedicine formulation that integrates activity-preserving immobilization, improved biological stability, and intracellular enzyme delivery. By enabling GaOX-mediated *in situ* H_2O_2 generation in the presence of D-galactose, this platform provides a formulation strategy for enhancing the functional performance of ROS-generating enzymes in cancer-related biomedical applications.

Conclusion

Efficient intracellular delivery of functional enzymes remains a major challenge for enzyme-based biomedical applications. In this study, we developed F127@nGO-GaOX as a nanographene oxide-based enzyme formulation platform for stabilizing and delivering galactose oxidase (GaOX). GaOX was physically immobilized onto nGO and subsequently coated with Pluronic F127, resulting in high enzyme loading, improved colloidal stability, and enhanced enzyme stability under biologically relevant conditions. Importantly, immobilized GaOX preserved its secondary structure, catalytic activity, and substrate affinity compared with the free enzyme. The F127@nGO-GaOX nanoplatform enabled efficient intracellular delivery of GaOX into cancer cells and induced D-galactose-dependent H_2O_2 generation, leading to enhanced oxidative stress and cytotoxicity. Overall, this study presents a simple nanocarrier-based formulation strategy for improving oxidase stability and intracellular delivery, supporting the potential of GaOX-based formulations for ROS-generating biomedical applications.

Author contributions

Junyoung Jung: Writing – original draft, Methodology, Investigation, Formal analysis, Visualization. **Abhishek Sahu**: Writing – original draft, Methodology, Investigation, Formal analysis, Visualization. **Giyoong Tae**: Supervision, Conceptualization, Writing – review & editing.

Conflicts of interest

There are no conflicts to declare

Data availability

The data supporting this article have been included as part of the Supplementary Information.

Acknowledgements

This research was financially supported by the National Research Foundation of Korea (NRF), funded by MSIT of Korea (RS-2025-00514481).

References

1 U. T. Bornscheuer, G. W. Huisman, R. J. Kazlauskas, S. Lutz, J. C. Moore and K. Robins, *Nature*, 2012, **485**, 185–194.
2 S. Ghosh, S. Alam, A. S. Rathore and S. K. Khare, in *Therapeutic Enzymes: Function and Clinical Implications*, ed. N. Labrou, Springer Singapore, Singapore, 2019, vol. 1148, pp. 131–150.
3 S. B. Ebrahimi and D. Samanta, *Nat Commun*, 2023, **14**, 2411.
4 K. Ji, L. Mayernik, K. Moin and B. F. Sloane, *Cancer Metastasis Rev*, 2019, **38**, 103–112.
5 R. Ramachandran, C. Altier, K. Oikonomopoulou and M. D. Hollenberg, *Pharmacological Reviews*, 2016, **68**, 1110–1142.
6 E. S. Radisky, *Journal of Biological Chemistry*, 2024, **300**, 107347.
7 F. M. Veronese and G. Pasut, *Drug Discovery Today*, 2005, **10**, 1451–1458.
8 J. Fang, T. Sawa, T. Akaike and H. Maeda, *Cancer Res*, 2002, **62**, 3138–43.
9 F. M. Veronese and A. Mero, *BioDrugs*, 2008, **22**, 315–329.
10 M. Sharifi, A. Y. Karim, N. Mustafa Qadir Nanakali, A. Salihi, F. M. Aziz, J. Hong, R. H. Khan, A. A. Saboury, A. Hasan, O. K. Abou-Zied and M. Falahati, *Journal of Biomolecular Structure and Dynamics*, 2020, **38**, 2746–2762.
11 M. N. Gupta, M. Kaloti, M. Kapoor and K. Solanki, *Artificial Cells, Blood Substitutes, and Biotechnology*, 2011, **39**, 98–109.
12 C. Ren, H. Liu, F. Lv, W. Zhao, S. Gao, X. Yang, Y. Jin, Y. Tan, J. Zhang, X. J. Liang and Z. Li, *ACS Appl Mater Interfaces*, 2020, **12**, 34667–34677.
13 J. Zhang, F. Zhang, H. Yang, X. Huang, H. Liu, J. Zhang and S. Guo, *Langmuir*, 2010, **26**, 6083–6085.
14 A. Soozanipour and A. Taheri-Kafrani, in *Methods in Enzymology*, Elsevier, 2018, vol. 609, pp. 371–403.
15 H. Seelajaroen, A. Bakandritsos, M. Otyepka, R. Zbořil and N. S. Sariciftci, *ACS Appl. Mater. Interfaces*, 2020, **12**, 250–259.
16 S. Goenka, V. Sant and S. Sant, *Journal of Controlled Release*, 2014, **173**, 75–88.
17 A. Sahu, W. I. Choi, J. H. Lee and G. Tae, *Biomaterials*, 2013, **34**, 6239–6248.
18 A. Sahu, K. Min, J. Jeon, H. S. Yang and G. Tae, *Journal of Controlled Release*, 2020, **326**, 442–454.
19 M. Wang, D. Wang, Q. Chen, C. Li, Z. Li and J. Lin, *Small*, 2019, **15**, 1903895.
20 L.-H. Fu, C. Qi, J. Lin and P. Huang, *Chem. Soc. Rev.*, 2018, **47**, 6454–6472.
21 W. Zhao, J. Hu and W. Gao, *ACS Appl. Mater. Interfaces*, 2017, **9**, 23528–23535.
22 P. Kanyong, F. D. Krampa, Y. Aniweh and G. A. Awandare, *Microchim Acta*, 2017, **184**, 3663–3671.
23 L. Wang, J. Li, D. Zhang, S. Ma, J. Zhang, F. Gao, F. Guan and M. Yao, *RSC Adv.*, 2020, **10**, 2870–2876.
24 J. Vilím, T. Knaus and F. G. Mutti, *Angew Chem Int Ed*, 2018, **57**, 14240–14244.
25 S. Supekar, D. W. P. Tay, W. L. Yeo, K. W. E. Tam, Y. S. Koo, J. Y. See, J. M. T. Miyajima, S. Maurer-Stroh, E. L. Ang, Y. H. Lim and H. Fan, *ACS Catal.*, 2024, **14**, 17233–17243.
26 K. Parikka, A.-S. Leppänen, L. Pitkänen, M. Reunanen, S. Willför and M. Tenkanen, *J. Agric. Food Chem.*, 2010, **58**, 262–271.
27 C. Jang, J. H. Lee, A. Sahu and G. Tae, *Nanoscale*, 2015, **7**, 18584–18594.
28 R. Paukner, P. Staudigl, W. Choosri, D. Haltrich and C. Leitner, *Protein Expression and Purification*, 2015, **108**, 73–79.
29 H. J. Wiggers, J. Cheleski, A. Zottis, G. Oliva, A. D. Andricopulo and C. A. Montanari, *Analytical Biochemistry*, 2007, **370**, 107–114.
30 S. Shamsi, A. A. Alagan, S. N. E. Sarchio and F. Md Yasin, *IJN*, 2020, **Volume 15**, 8311–8329.
31 M. Aziz, F. S. Abdul Halim and J. Jaafar, *Jurnal Teknologi*, DOI:10.11113/jt.v69.3388.
32 B. Karolewicz, A. Górniak, A. Owczarek, E. Żurawska-Płaksej, A. Piwowar and J. Pluta, *J Therm Anal Calorim*, 2014, **115**, 2487–2493.
33 F. Zhao, H. Li, Y. Jiang, X. Wang and X. Mu, *Green Chem.*, 2014, **16**, 2558.
34 N. Ranjbari, M. Razzaghi, R. Fernandez-Lafuente, F. Shojaei, M. Satari and A. Homaei, *International Journal of Biological Macromolecules*, 2019, **130**, 564–572.
35 M. Besharati Vineh, A. A. Saboury, A. A. Poostchi, A. M. Rashidi and K. Parivar, *International Journal of Biological Macromolecules*, 2018, **106**, 1314–1322.
36 J. W. Whittaker, *Archives of Biochemistry and Biophysics*, 2005, **433**, 227–239.
37 S. Savino and M. W. Fraaije, *Biotechnology Advances*, 2021, **51**, 107634.
38 M. Royvaran, A. Taheri-Kafrani, A. Landarani Isfahani and S. Mohammadi, *Chemical Engineering Journal*, 2016, **288**, 414–422.
39 M. Monajati, S. Borandeh, A. Hesami, D. Mansouri and A. M. Tamaddon, *Chemical Engineering Journal*, 2018, **354**, 1153–1163.
40 P. Bolibok, M. Wiśniewski, K. Roszek and A. P. Terzyk, *Sci Nat*, 2017, **104**, 36.
41 R. Böttger, R. Hoffmann and D. Knappe, *PLoS ONE*, 2017, **12**, e0178943.
42 S. Hermanová, M. Zarevúcká, D. Bouša, M. Pumera and Z. Sofer, *Nanoscale*, 2015, **7**, 5852–5858.

View Article Online
DOI: 10.1039/D6PM00162A

43 R. A. Sheldon and S. Van Pelt, *Chem. Soc. Rev.*, 2013, **42**, 6223–6235.
44 J. Huang, C. Zong, H. Shen, M. Liu, B. Chen, B. Ren and Z. Zhang, *Small*, 2012, **8**, 2577–2584.
45 Q. Mu, G. Su, L. Li, B. O. Gilbertson, L. H. Yu, Q. Zhang, Y. P. Sun and B. Yan, *ACS Appl Mater Interfaces*, 2012, **4**, 2259–66.
46 Z. Xu, S. Wang, Y. Li, M. Wang, P. Shi and X. Huang, *ACS Appl. Mater. Interfaces*, 2014, **6**, 17268–17276.
47 F. Yan, C. Zhang, Y. Zheng, L. Mei, L. Tang, C. Song, H. Sun and L. Huang, *Nanomedicine*, 2010, **6**, 170–8.
48 F. Himo, L. A. Eriksson, F. Maseras and P. E. M. Siegbahn, *J. Am. Chem. Soc.*, 2000, **122**, 8031–8036.
49 H. Nakamura and K. Takada, *Cancer Science*, 2021, **112**, 3945–3952.
50 B. Perillo, M. Di Donato, A. Pezone, E. Di Zazzo, P. Giovannelli, G. Galasso, G. Castoria and A. Migliaccio, *Exp Mol Med*, 2020, **52**, 192–203.

View Article Online
DOI: 10.1039/D6PM00162A

Data availability

The data supporting this article have been included as part of the Supplementary Information.